Miniaturization and defocus correction for objective-coupled planar illumination microscopy

Diwakar Turaga and Timothy E. Holy*

Department of Anatomy and Neurobiology, Washington University in St. Louis School of Medicine, 660 S. Euclid, St. Louis, Missouri 63110, USA

**Corresponding author: holy@wustl.edu*

Received July 17, 2008; accepted August 14, 2008;
posted August 29, 2008 (Doc. ID 98349); published October 7, 2008

Recently, a light sheet-based technique called objective-coupled planar illumination (OCPI) microscopy [Holekamp *et al.*, Neuron **57**, 661 (2008)] was shown to permit low-phototoxicity, high-speed, three-dimensional fluorescence imaging of extended tissue samples. Here, we introduce two major improvements in OCPI microscopy. First, we miniaturize the objective coupler by using a uniaxial gradient-index lens to produce the light sheet. Second, we demonstrate theoretically and experimentally that refractive index mismatch at the fluid/tissue interface causes a significant defocus aberration. By introducing the ability to tune the angle of the light sheet, we show that defocus correction in a miniaturized OCPI microscope leads to a significant improvement in image sharpness deeper into tissue. © 2008 Optical Society of America

OCIS codes: 180.2520, 180.6900, 110.2760, 170.3660, 170.2945, 170.3880.

Epifluorescence microscopy and laser scanning (confocal and multiphoton) fluorescence microscopy have become indispensable tools in biology, but each of these techniques has a fundamental limitation. Epifluorescence has little depth resolution and thus encounters difficulty when imaging thick samples. Laser scanning microscopy, with its sequential pixel scanning, encounters a fundamental trade-off among speed, imaged area, and signal-to-noise ratio [1].

One approach to overcome these limitations is planar illumination microscopy [1–6]. A thin sheet of light (typically formed with a cylindrical lens) is projected from the side and positioned to illuminate the focal plane of the objective, exciting fluorescence only in the in-focus portion of the sample. This achieves optical sectioning and eliminates photodamage in out-of-focus regions of the sample. Moreover, because emission from all illuminated points can be collected simultaneously, this approach permits entire images to be collected quickly at high signal-to-noise ratios. High speed and low phototoxicity are essential for imaging fast events, such as electrical activity in large populations of neurons [1].

In our implementation of planar illumination, objective-coupled planar illumination (OCPI) [1], the light sheet is rigidly coupled to the objective so that both can be rapidly translated together to attain fast three-dimensional imaging. In this Letter we report improving OCPI by (1) miniaturizing the objective laser coupler and (2) correcting defocus aberrations that arise from refractive index mismatch.

In this new implementation of OCPI, we reduce the optical requirements to a single component: a uniaxial (cylindrical) gradient-index (GRIN) lens. A GRIN lens bends light by having an index of refraction n that is highest in the center and falls off quadratically toward the edge, $n=n_0[1-(gy)^2]$, where n_0 is the index of refraction at the center, y is the distance from the center, and g measures how quickly the refractive index changes with distance [7]. We employ a slab-shaped GRIN lens whose index of refraction varies only along one axis (as opposed to typical GRIN lenses whose n changes radially), thus behaving as a cylindrical lens. The custom GRIN lens (GRINTECH GmbH, thickness 1 mm, width 3 mm, length 2.66 mm, $n_0=1.524$, $g=0.26/\text{mm}$, working distance of 3.5 mm in water) is mounted on a custom objective collar that permits micropositioning of the light sheet [Fig. 1(a)].

The thickness of the light sheet over the field of view is determined by tuning the NA of the GRIN lens [1] using a slit at the rear aperture. In our current implementation, a 488 nm laser (Coherent 488-20) directly illuminates the back aperture of the GRIN lens to give a diffraction-limited light sheet with a waist of 3–5 μm thick across a field hundreds of micrometers in size [Fig. 1(c)]. Light collected by the objective (Olympus, 20× water immersion, NA 0.5) is focused by a 200 mm tube lens (Edmund Optics) onto a CCD camera (Scion CFW–1308). This configuration of using uniaxial GRIN lens with free

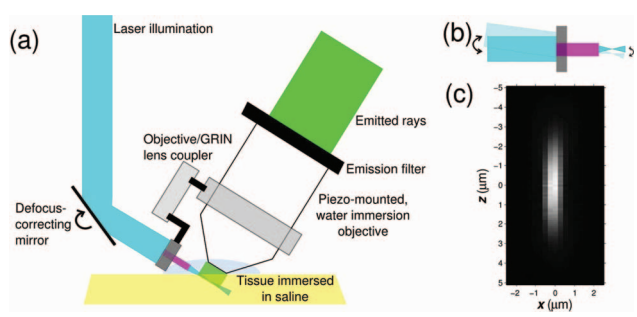

Fig. 1. Schematic and calibration of OCPI microscope. (a) Schematic of miniaturized objective coupler. Uniaxial GRIN lens is positioned such that a sheet of light is formed at the focal plane of the objective. (b) Angular defocus adjustment is obtained by changing the angle of incident light. (c) Example axial image of a 0.2 μm fluorescent bead in agar.

 © 2008 Optical Society of America

space laser coupling leads to a substantial decrease in bulk of the illumination arm compared with our previous design [1], permitting a wider range of samples to be imaged.

OCPI images of tissue are degraded in part by scattering, which arises from inhomogeneities in the refractive index of the sample. However, image quality is also affected by low-order aberrations that arise from bulk index mismatch: the immersion fluid has a refractive index $n_f = 1.33$, while the tissue sample typically has an average refractive index $n_s \approx 1.36-1.40$ [8].

To study the consequences of this index mismatch, we calculated the refraction of meridional paraxial rays under the idealization of an optically homogeneous tissue sample. We assumed that the interface between two homogenous media, fluid and sample, is planar, with the normal vector at an angle α with respect to the optic axis [Fig. 2(a)]. Suppose also that we idealize the incident illumination as a plane, which is at an angle β with respect to the optic axis, and that the normal of the illumination plane lies in the same plane as the sample normal and the optic axis. Using Snell's law and assuming that the difference $\Delta n = n_s - n_f$ is small, the illumination bends by an angle $\theta_i \approx -(\Delta n / n_f) \tan \gamma_s$, where γ_s is the angle between the interface normal and the light sheet inside the sample [Fig. 2(b)]. So if the illumination plane coincides with the focal plane in the fluid, the two will not remain coincident in the sample, with the separation increasing deeper into the sample.

However, the total defocus also must account for a second phenomenon, the deviation of the emitted (collected) rays at the fluid/sample interface [Fig. 2(c)]. Paraxial rays emitted from one object location O will appear to be emitted from a virtual source O' whose position can be determined by backtracing the rays in the fluid. Consider two meridional rays emitted at angles $\pm\epsilon$ from the optic axis. These two rays strike the interface and are refracted according to

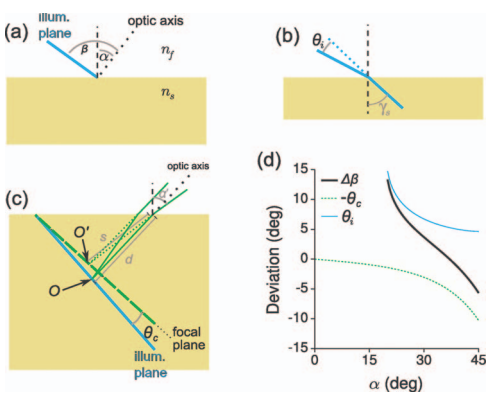

Fig. 2. Sources and magnitude of defocus in tilted configurations of planar illumination microscopy. (a) Illumination strikes the sample/fluid interface at an angle; the optic axis is also tilted, at an angle α. The fluid has an index of refraction n_f, the sample n_s. (b) Illumination plane bends at the fluid/sample interface through an angle θ_i. (c) Emitted rays are bent at the interface, resulting in a virtual object location that resides on a different plane. (d) Magnitude of both effects, and their combination ($\Delta\beta$), for $n_f = 1.33$ and $n_s = 1.40$.

Snell's law. Denote the separation between their interface strike positions by $\Delta\mathbf{x}$, and the difference in their refracted angles by $\Delta\theta$; in terms of these quantities, using the law of sines one can show that (to lowest order in ϵ) the backtraced rays intersect at a distance $s = \cos\alpha' |\Delta\mathbf{x}| / \sin(\Delta\theta)$ along the rays, where α' is the angle between the interface normal and the refracted axial ray. A short calculation shows that, to lowest order, $|\Delta\mathbf{x}| = 2\epsilon d / \cos\alpha$ and $\Delta\theta = 2\epsilon(n_s/n_f) \cos\alpha / \cos\alpha'$, yielding $(s = d n_f \cos^2\alpha')/(n_s \cos^2\alpha)$. (This generalizes the familiar fact from face-on imaging, $\alpha = \alpha' = 0$, that in the paraxial limit the object appears to be at a depth $s = d n_f / n_s$.) Thus, the apparent position shift of the object is $\Delta z = d - s \cos(\alpha' - \alpha)$ and $\Delta y = s \sin(\alpha' - \alpha)$, where z measures along the optic axis and y along the meridian. Note in particular that the deviation is linear in d, which means that for objects O in the illumination plane, the virtual origins O' also lie in a plane, but one that is tilted with respect to the illumination [Fig. 2(c)].

To correct the defocus of emitted rays, we need to ensure that the *virtual* source plane (rather than the illumination plane) lies in the focal plane of the imaging system [Fig. 2(c)]. The illumination plane must therefore be tilted at an angle θ_c relative to the focal plane (the plane perpendicular to the optic axis). This angle is determined by the requirement that the position shift Δz for each illuminated point places it along a line perpendicular to the optic axis. For small Δn one finds

$$\tan\theta_c \approx \frac{\Delta n}{n_f}(1 + 2\tan^2\alpha)\tan\alpha. \qquad (1)$$

Figure 2(d) shows the combined effect of the deviation of the illumination plane [Fig. 2(b)] and of the deviation of the emitted rays [Fig. 2(c)] in setting the ideal illumination angle [Fig. 2(a)] $\beta = \pi/2 + \Delta\beta$, where theoretically $\Delta\beta = \theta_i - \theta_c$.

Thus there is a small angular change ($\Delta\beta$) required to ensure that the illumination plane is properly positioned for the objective. By placing a mirror on a rotation stage (Thorlabs), we were able change the angle of incident laser onto the back aperture of the GRIN lens to produce the required few degrees change in the illumination angle [Fig. 1(b)].

To test the effect of angular defocus, we imaged 0.2 μm fluorescent beads in water ($n = 1.33$) and polydimethylsiloxane (PDMS, Dow Corning, DC 184-A and DC 184-B with a weight ratio of 10:1, $n = 1.40$). When imaging beads in water (10 ms exposure time to limit the effects of diffusion), we tuned for the angle that produced the least defocus aberration throughout the imaged plane. This setting corresponds to the illumination axis being orthogonal to the objective axis (thus under our definition $\Delta\beta = 0°$) [Fig. 3(a)]. Under the same angular setting, beads in PDMS were increasingly blurry at increasing depths [Fig. 3(b)], as expected theoretically (Fig. 2).

We then tuned the illumination to find the optimum angle (determined experimentally as $\Delta\beta \approx 5.4°$)

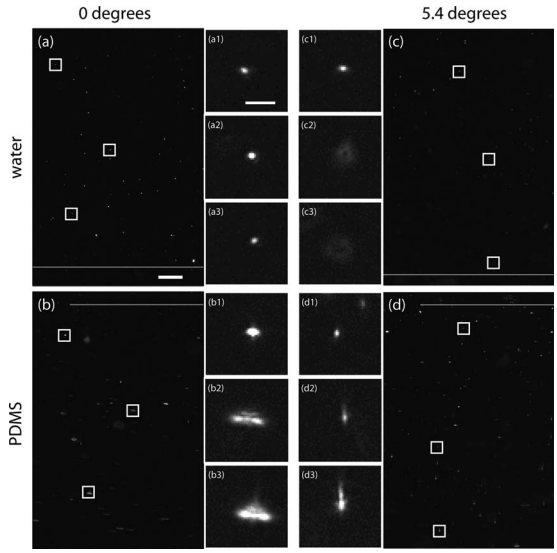

Fig. 3. Defocus measurement. (a) Beads in water ($n=1.33$) were imaged under OCPI. At this illumination angle, the image of beads is diffraction limited. Insets are three different beads at three corresponding depths. The dotted line represents water/PDMS interface. (b) Beads in PDMS ($n=1.40$) at same angle as (a). As expected, as depth increases, the defocus increases. (c) Beads in water. At an angle tuned for beads in PDMS, the beads in water are increasingly defocused as the depth increases. (d) Beads in PDMS at the same angle as (c). Although there are some higher-order aberrations, the beads are in focus at all depths. Scale bar in (a), 25 μm. Scale bar in (a1), 5 μm.

that minimized defocus aberration in beads embedded in PDMS [Fig. 3(d)]. At such an angle the beads in PDMS were adequately in focus across the field of view, with small defects in image quality from uncorrected higher-order aberrations. At this new angle, as expected, the beads immersed in water were considerably out of focus at increasing distance [Fig. 3(c)]. The 5.4° corresponds well with the theoretical prediction [Fig. 2(d)] of 3° for $\alpha=30°$.

To see the net improvement of the miniaturized OCPI with defocus correction, we imaged a slice of olfactory bulb from a GAD65-GFP mouse [9]. A 500-μm-thick tissue section was imaged under the old and new OCPI microscopes (Fig. 4). Since the refractive index of the tissue is unknown, we empirically tuned the illumination angle, which for this sample was optimized at $\Delta\beta \approx 3.4°$. The new OCPI microscope provides substantially better images

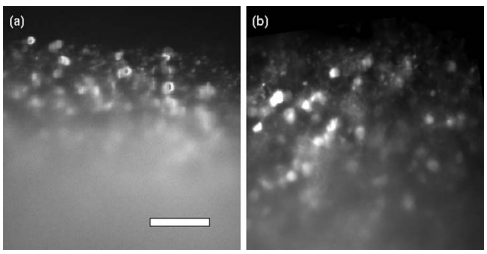

Fig. 4. Resolution enhancement with miniaturized objective coupler with defocus correction. Images of a slice of olfactory bulb were taken under the same conditions with (a) old and (b) new OCPI microscopes. Scale bar, 50 μm.

deeper into tissue; remaining loss of sharpness with depth is due to a combination of scattering and uncorrected classical aberrations [as seen in Fig. 3(d)]. These remaining aberrations might be corrected by other methods, including adaptive optics, which should lead to even greater improvement in image sharpness deeper into tissue.

The authors thank John Kreitler and Charlie Hamontree for machining the coupler, Julian Meeks for preparing olfactory bulb slices and machining, Zhongsheng Guo for designing the acquisition software, and Adam Puche and Gábor Szabó for GAD65-GFP mice. This research was funded by a McKnight Technological Innovation in Neuroscience award (T. E. Holy).

References

1. T. F. Holekamp, D. Turaga, and T. E. Holy, Neuron **57**, 661 (2008).
2. H. Siedentopf and R. Zsigmondy, Ann. Phys. **10**, 1 (1903).
3. A. H. Voie, D. H. Burns, and F. A. Spelman, J. Microsc. **170**, 229 (1993).
4. E. Fuchs, J. S. Jaffe, R. A. Long, and F. Adam, Opt. Express **10**, 145 (2002).
5. J. Huisken, J. Swoger, F. Del Bene, J. Wittbrodth, and E. H. K. Stelzer, Science **31**, 1007 (2004).
6. H.-U. Dodt, U. Leischner, A. Schierloh, N. Jahrling, C. P. Mauch, K. Deininger, J. M. Deussing, M. Eder, W. Zieglgansberger, and K. Becker, Nat. Methods **4**, 331 (2007).
7. J. C. Jung, A. D. Mehta, E. Aksay, R. Stepnoski, and M. J. Schnitzer, J. Neurophysiol. **92**, 3121 (2004).
8. J. J. Dirckx, L. C. Kuypers, and W. F. Decraemer, J. Biomed. Opt. **10**, 44014 (2005).
9. G. Lopez-Bendito, K. Sturgess, F. Erdélyi, G. Szabó, Z. Molnar, O. Paulsen, Cereb. Cortex **14**, 1122 (2004).